Launching Coherent Acoustic Phonon Wave Packets with Local Femtosecond Coulomb Forces

Shaoxiang Sheng,[1,*] Anne-Catherine Oeter,[1] Mohamad Abdo,[1,2] Kurt Lichtenberg,[1] Mario Hentschel,[3] and Sebastian Loth[1,2,†]

[1]University of Stuttgart, Institute for Functional Matter and Quantum Technologies, 70569 Stuttgart, Germany
[2]Max Planck Institute for Solid State Research, 70569 Stuttgart, Germany
[3]University of Stuttgart, 4th Physics Institute and Research Center SCoPE, 70569 Stuttgart, Germany

(Received 15 February 2022; accepted 22 June 2022; published 18 July 2022)

Generation and manipulation of coherent acoustic phonons enables ultrafast control of solids and has been exploited for applications in various acoustic devices. We show that localized coherent acoustic phonon wave packets can be launched by ultrafast Coulomb forces in a scanning tunneling microscope (STM) using tip-enhanced terahertz electric fields. The wave packets propagate at the speed of the longitudinal acoustic phonon, creating standing waves up to 0.26 THz for a 6.4 nm thin Au film on mica. The ultrafast lattice displacement can be as large as 5 pm and is precisely controlled by varying the tip-sample distance. This nonthermal femtosecond Coulomb-force-based excitation mechanism is applicable in nano-optomechanics for advanced terahertz engineering and opens new perspectives in exploiting coherent phonons at the atomic scale.

DOI: 10.1103/PhysRevLett.129.043001

Coherent acoustic phonon (CAP) waves—the collective motion of atoms—propagate on the surface and inside of solids with low losses and over long distances [1,2]. They can create a propagating potential landscape [3] that transiently reshapes material properties [4–9]. CAPs also excite spin waves [10,11], and can be used for quantum information processing as their wavelength is much shorter than electromagnetic waves at comparable frequencies [12,13], making it desirable to spatially control and detect CAPs on the nanometer scale.

Detection of high-energy optical phonons at this length scale has been achieved in STM by tip-enhanced Raman scattering [14,15] and inelastic electron tunneling [16], and vibrations of individual molecules can be controlled dynamically by terahertz-coupled STM [17,18]. By contrast, atomic-scale control over the low-energy acoustic phonons remains elusive.

On length scales of hundreds of nanometers, laser pulses excite CAPs with bandwidth up to terahertz frequencies. As CAPs do not couple directly to light, indirect excitation mechanisms such as thermoelasticity and electronic pressure through the electron deformation potential [19] were used. However, those are challenging to port to length scales significantly below the laser wavelength.

In this Letter, we use single-cycle terahertz pulses to excite CAP wave packets directly by coupling the terahertz electric field to the sample surface via the asperity of the STM tip, Fig. 1(a). The field enhancement at the tunnel junction creates a strong transient electric field [20,21] with induced charges on the tip and the sample surface. These charges result in an ultrafast attractive Coulomb force between tip and surface that lasts less than a picosecond. This force pulse displaces the surface atoms impulsively and launches a strain wave into the sample. By using a thin film of gold on mica, the strain wave is repeatedly reflected at the buried gold-mica interface and the sample surface creating a characteristic periodic beating of the surface.

We use pairs of terahertz pulses [18,21–23] to resolve the ultrafast surface motion. The STM tip is approached into tunneling distance to the atomically flat Au surface [Fig. 1(b)] and terahertz pulses are focused on the STM tip. The terahertz-induced tunnel current scales with the junction conductance at the time of the terahertz pulse, and therefore modulates with the ultrafast surface displacement. Both pulses used in our experiment are of equal magnitude, hence both induce tunneling current and force pulses. The tunnel current of the trailing pulse measures the ultrafast surface displacement caused by the transient force of the preceding pulse and therefore modulates with the delay between the pulses. By contrast, the tunnel current induced by the preceding pulse is delay independent, as it encounters the surface at rest. We selectively detect the tunnel current of the trailing pulse by using lock-in detection upon chopping the pulse on and off (see Supplemental Material, Methods [24]). Then, slowly sweeping the delay between both pulses measures a time trace of the ultrafast variations in the tunnel current, Fig. 1(d).

We restrict our analysis to positive delays where the chopped pulse (termed probe pulse) follows the non-chopped pulse (termed pump pulse). When both pulses overlap at 0 ps time delay, the terahertz-induced tunnel current peaks to 35 pA and quickly drops to 1.2 pA for time

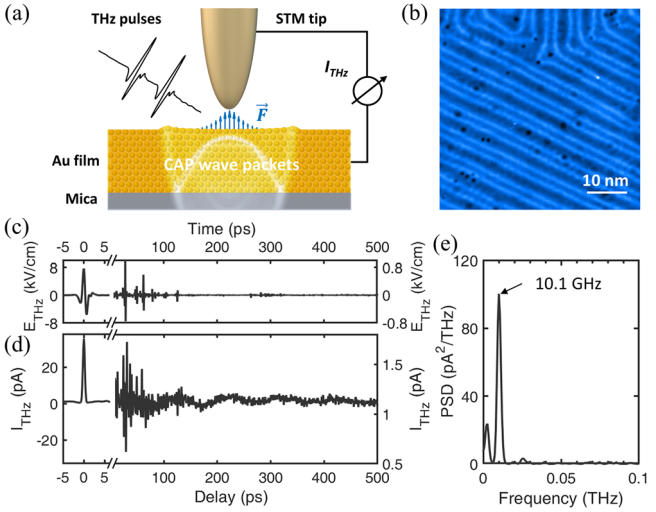

FIG. 1. (a) Schematic of the terahertz pulses (black) launching acoustic phonon wave packets (white) in a Au film (yellow) on mica (gray) under the STM tip. (b) Constant current topography of the atomically flat Au(111) surface. (c) Terahertz electric field waveform E_{THz} measured by electro-optic sampling. Minor peaks at 28 to 60 ps stem from reflections of the terahertz pulse at cryostat windows and tip holder. (d) Time-resolved terahertz-induced tunnel current I_{THz} measured on a Au film of $151\ \mathrm{nm} \pm 12\ \mathrm{nm}$ thickness showing long-period oscillations. (e) Fast Fourier transform of the time trace shown in (d) from 3 to 500 ps. Tunnel junction set point 100 pA at 30 mV.

delays larger than 2 ps when pump and probe no longer overlap, Fig. 1(d). Remarkably, the current undergoes periodic oscillations (∼100 ps) with an amplitude of 93 fA that can be observed for at least 500 ps after the pump pulse. The fast Fourier transform (FFT) of the oscillatory part of the time trace shows a prominent peak at 10.1 GHz, Fig. 1(e).

This oscillation must originate from the Au sample as it is absent in the terahertz pulse's electric field waveform, Fig. 1(c). The Au film is measured to have a thickness of 151 ± 12 nm by focused ion beam (FIB) cross section in scanning electron microscopy, Fig. S1 [24]. The observed frequency of 10.1 GHz matches well to the fundamental standing wave mode of the longitudinal acoustic phonon in this film (10.8 ± 0.9 GHz, Fig. S1). Therefore, we infer that the measured long-period oscillation originates from CAP wave packets bouncing back and forth between the gold surface and the gold-mica interface thereby creating a periodic displacement of the surface.

The period of these oscillations should depend on the thickness of the Au film. Hence, repeated sputtering cycles were carried out to reduce the film thickness controllably (see Supplemental Material, Methods [24]). The resulting FFT spectra show a blueshift of the frequency as the film thickness decreases [Fig. 2(a)], reaching 260 GHz for the thinnest film of 6.4 nm. The thickness dependence is fit quantitatively by the function $f_{\mathrm{CAP}} = v/2H$ that describes the fundamental frequency, f_{CAP}, of a phonon echo in a film

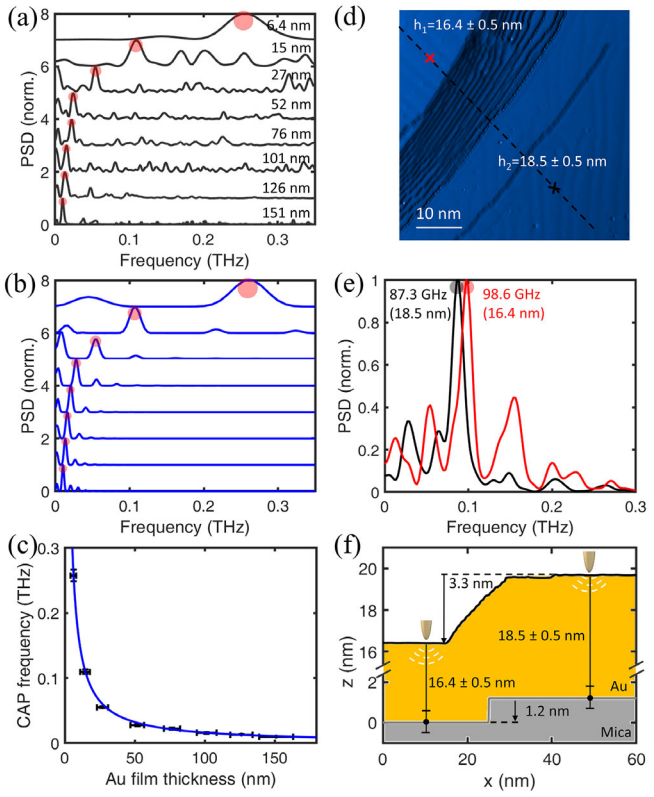

FIG. 2. (a) Power spectral density, PSD, of terahertz tunnel current time traces measured on Au films with thicknesses ranging from 6.4 to 151 nm. Red dots mark the CAP echo frequency. Spectra normalized to a span of 1 and offset vertically for clarity. (b) PSD of calculated time traces obtained from the discrete lattice phonon propagation model for the Au film thicknesses of (a) (see Fig. 3, Table S1 and Supplemental Material, Methods [24] for details). (c) CAP echo frequency, f_{CAP}, as a function of film thickness H extracted from (a) (dots) and fit for the echo frequency $f_{\mathrm{CAP}} = v/2H$ (blue curve). Error bars indicate experimental uncertainty in film thickness and measurement accuracy in frequency. (d) Gradient STM topography of an area of the Au surface that features multiple steps. (e) PSD of time traces recorded with STM tip at either side of the Au surface steps marked by crosses in (d). (f) Height profile (black line) along the dashed line in (d) and gold-mica interface position (black dots) determined from CAP echo frequencies in (e). Colored areas (orange, gray) depict thin film cross section. Tunnel junction set point 100 pA at 1 V.

of thickness H when the velocity of propagation is v, Fig. 2(c). By using the film thickness determined by FIB cross section and the material removal during sputtering, the fit to the measured frequencies yields $v = 3235 \pm 67$ m/s. This matches to the literature value of the sound velocity of the longitudinal acoustic phonon in gold [26], confirming that the observed oscillations originate from terahertz-induced CAP wave packets propagating throughout the Au film.

An area of the Au surface that features multiple atomic steps, Fig. 2(d), can be used to highlight that this CAP wave

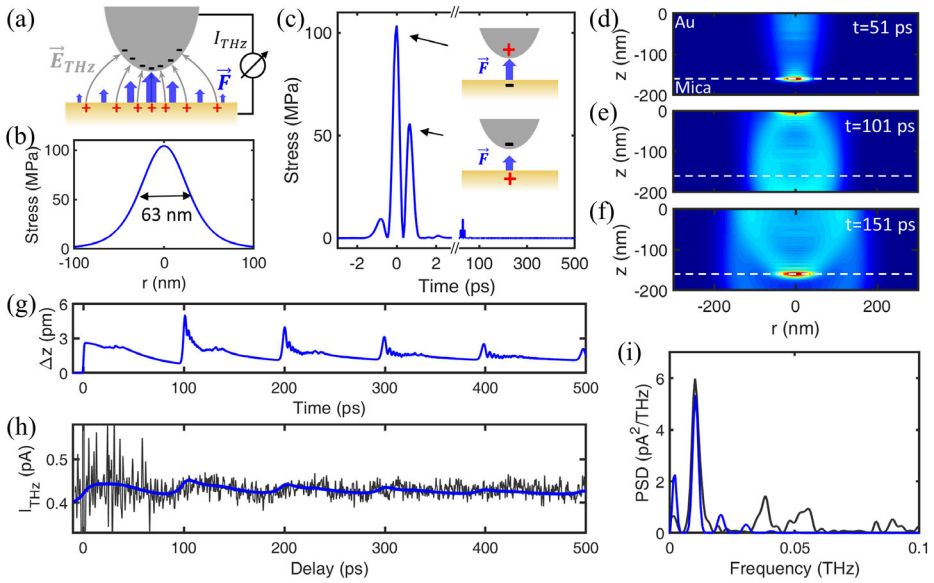

FIG. 3. (a) Sketch of the ultrafast Coulomb force F (blue) acting on the gold surface. The electric field of the terahertz pulses, E_{THz} (gray arrows), induces charges (+ and −) on the sample (yellow) and tip surface (gray) that attract each other. (b) Distribution of the peak stress on the sample surface induced by the Coulomb force. (c) Waveform of the stress pulse induced by a terahertz pulse. The insets show the sign of induced charges and force direction in the tunnel junction at $t = 0$ ps and 0.7 ps. (d)–(f) Propagation of the CAP wave packets as function of lateral position r from tip apex and depth beneath the Au surface z, calculated with the discrete lattice phonon propagation model at time t after the excitation pulse. Color shows strain from 0 pm (blue) to 5 pm (red). (g) Ultrafast surface displacement under the STM tip induced by the Coulomb stress pulse shown in (b) and (c). (h) Measured (black) and calculated (blue) time trace of terahertz-induced tunnel current as function of delay after the excitation pulse for $\Delta z(t)$ of (g). Tunnel junction set point 100 pA at 1 V. (i) PSD of the measured (black) and calculated (blue) time traces in (h).

packet excitation is highly localized. Spectra recorded at either side of the Au surface step show the phonon echo frequency to change from 87.3 ± 2.2 GHz to 98.6 ± 2.3 GHz, Fig. 2(e). By using the speed of the longitudinal phonon determined above, the film thickness can be determined to 16.4 ± 0.5 nm at the lower side (red cross) and 18.5 ± 0.5 nm at the higher side (black cross) of the surface step, Fig. 2(d). Since the step visible at the surface is 14 layers of Au high (3.3 nm), we can infer that the surface step must coincide with a step at the buried Au-mica interface of 1.2 ± 0.5 nm height, Fig. 2(f). This height matches with the height of a single layer step in mica [37]. This measurement shows a lateral spatial resolution better than 40 nm, indicating that the tip-induced phonon excitation can be used as a nanosonar for detection of buried interfaces.

To explain the mechanism by which the terahertz pump pulse launches a CAP wave packet into the sample, we consider the interaction of the terahertz electric field with the tunnel junction. Millimeter-scale optical experiments observed ultrafast Joule heating via terahertz-driven screening currents in metal films [33,34]. Despite the strong field enhancement at the STM tip, this effect is insufficient to produce the large surface displacement observed here. We estimate that the lattice temperature increase is only 1 mK (see Supplemental Material, Note S1 [24]), because of low electron-phonon coupling and ultrafast diffusion of hot electrons in gold films [19]. By contrast, a lattice temperature increase of approximately 50 K would be required to create the observed surface displacement by Joule heating [36]. Hence, a nonthermal excitation mechanism must be active in the tunnel junction.

In general, any electric field between tip and sample displaces charges to the tip apex and sample surface through electrostatic induction [27,38]. This creates the local field enhancement and also causes the atoms in the tip and sample surface to carry a net charge. As a result, the electric field exerts a Coulomb force on the surface atoms, Fig. 3(a). This is the working principle of electrostatic force microscopy [27] and we extend it here to terahertz frequencies.

The terahertz pulses add a strong transient electric field [20] that redistributes the induced charges and therefore causes an ultrafast modulation of the Coulomb force. It is worth noting that this effect would not occur on a charge-neutral Au surface in the absence of a tip. In the quasistatic limit for terahertz frequencies significantly below the plasmon resonance of Au, the strength of the Coulomb force modulation can be estimated by the derivative of the electric potential energy with tip-sample distance z as $\Delta F_C = \frac{1}{2}(\partial C/\partial z)V_{\mathrm{THz}}^2$ [39], where C is the capacitance of the tunnel junction and V_{THz} is the terahertz-induced voltage which peaks to $5.0\ \mathrm{V} \pm 0.1\ \mathrm{V}$ in our experiment (see Supplemental Material, Note S2 [24]). Charge transfer

by the tunneling current can be neglected because it is several orders of magnitude smaller than the induced surface charge. For typical STM tips dC/dz is on the order of 6 aF/nm [40]. Thus, a Coulomb force pulse on the order of 75 nN is expected that acts on a nanometric region under the tip, Fig. 3(b). This force pulse will accelerate the surface Au atoms toward the tip and launch a CAP wave packet into the gold film.

We approximate the propagation of this phonon wave packet as a strain wave, and simulate it with a two-dimensional discrete lattice model (see Supplemental Material, Methods [24]). We find that the strain wave propagates through the gold film as an elongated spherical wave front because the longitudinal and transverse sound velocities differ, Fig. 3(d). The strain wave packet partially reflects at the buried Au-mica interface, propagates back to the surface, Fig. 3(e), reflects at the Au-vacuum interface and repeats the process, Fig. 3(f). Every reflection at the surface entails an additional movement of the surface atoms resulting in a time-dependent surface displacement $\Delta z(t)$ that features a characteristic series of echos of the strain wave packet, Fig. 3(g). The ultrafast surface displacement (excited by the pump pulse) is directly picked up by the probe pulse as a modulation of the terahertz-induced tunnel current (see Supplemental Material, Methods for details [24]).

We find that this minimalistic model achieves very good agreement with the measured ultrafast tunnel current modulation, Fig. 3(h), allowing us to extract echo periods and surface stress waveforms quantitatively.

The magnitude of the tunnel current modulation is best fit for a peak surface stress of 103 MPa, Fig. 3(c). This substantial stress displaces the gold surface by as much as 3 pm immediately after the pump pulse, Fig. 3(g). The observed decay of the echo amplitude with every reflection is well reproduced with a lateral extension of the stress pulse of 63 nm [Fig. 3(b)] and by assuming the phonon wave packet experiences no damping on the 500 ps time-scale, i.e., the echo decay originates solely from the transverse spreading of the wave packet and the partial transmission of phonons into the mica substrate.

The echo period is fit to the FFT spectrum, Fig. 3(i), and yields 160 ± 7 nm thickness. This matches within measurement uncertainty to the 151 ± 12 nm thickness obtained by the FIB cross section, Fig. S1. In addition, we find that the scaling of the main frequency of the phonon echoes is well reproduced in the calculated phonon propagation simply by using the average film thicknesses deduced from sputtering, Fig. 2(b).

The measured spectra feature additional peaks at higher frequencies that are not present in the calculated spectrum. These modes change significantly at different locations on the sample surface, Fig. S7, and may stem from longitudinal and transverse phonon wave packet reflections at spatial inhomogeneities of the film (see Supplemental Material, Note S3 [24]) that were not included in the model. This further signifies the possibility of using terahertz-coupled STM as a sonarlike tool for nanoscale material spectroscopy.

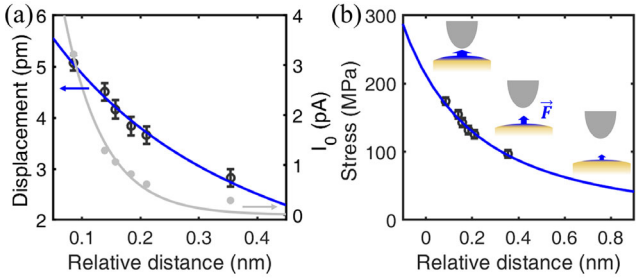

FIG. 4. (a) Peak surface displacement (left axis, black circles) and terahertz-induced tunnel current in the absence of surface motion I_0 (right axis, gray dots), measured as a function of relative tip-sample sample distance, d ($d = 0$ nm is given by tunnel junction set point 36 pA at 1 mV). The surface displacement fits with the decay behavior $\Delta z = a_0/(d + d_0)^2$ (blue curve) caused by the distance dependence of the electric field in the tunnel junction for $d_0 = 0.67 \pm 0.06$ nm, $a_0 = 2.85 \pm 0.40$ nm^3. I_0 fits to the expected exponential decay of the tunnel current, $I_0 = b_0 e^{-\kappa d}$ (gray curve), with $\kappa = 1.78 \pm 0.12$ Å^{-1} and $b_0 = 13.51 \pm 1.68$ pA. (b) Peak surface stress derived from the peak surface displacement in (a) (open circles) and fit to the expected behavior for ultrafast Coulomb force (blue curve) for an absolute tip-sample distance of 0.72 nm at the tunnel junction set point.

We find that the magnitude of the stress pulse, and hence the surface displacement, depend on the tip-sample distance d. Upon decreasing d by $\Delta d = 2.7$ Å, the surface displacement amplitude increases from 2.8 to 5.1 pm, Fig. 4(a). At the same time, the terahertz-induced tunnel current I_0 increases exponentially from 0.31 to 3.2 pA. The surface displacement fits to a $[1/(d_0 + \Delta d)^2]$ behavior, Fig. 4(a). This matches to the expected tip-surface distance dependence of a stress pulse caused by ultrafast Coulomb force: the Coulomb force acts on the induced charges making the stress proportional to the square of the electric field strength, and since the electric field strength in the tunnel junction scales as d^{-1} (V_{THz} is independent of d [20,31]), the stress scales as d^{-2}.

The scaling behavior highlights that the origin of the unexpectedly strong terahertz-induced Coulomb forces lies in the extreme enhancement of the electric field in the tunnel junction. It is possible to create strong localized stress pulses on the order of the tensile strength of many materials even with relatively weak terahertz pulses, Fig. 4(b). Extrapolating from the observed behavior shows that peak stresses on the order of 1–10 MPa would be reached even for tip-sample distances between 3 to 10 nm. The long-range nature of Coulomb force indicates that this excitation method is applicable in other scanning probe techniques, such as scattering scanning near-field optical microscopy [41].

In summary, tip-enhanced transient terahertz pulses can induce femtosecond Coulomb forces in an STM junction. The terahertz-induced Coulomb force features a bandwidth beyond 1 THz, as it is proportional to the square of the tip-enhanced terahertz electric field. These localized forces launch CAP wave packets into the sample. The resulting ultrafast surface displacement can reach up to 5 picometers with the amplitude being precisely controlled by varying the tip-sample distance. Phonon standing waves in a Au thin film are observable by terahertz-coupled STM for hundreds of picoseconds indicating negligible damping. This makes ultrafast Coulomb forces ideal for the excitation of acoustic phonons at the nanometer level and may boost spatial resolution in phonon nanoscopy imaging and diagnostics below surfaces. The nonthermal excitation by Coulomb forces may enable *in situ* phonon generation even in samples with delicate electronic phases [42,43].

The authors thank Stephan Spieker and Michael Schäfer for expert technical assistance. S. S. acknowledges a postdoctoral fellowship from the Alexander von Humboldt Foundation. This project has received funding from the European Research Council (ERC) under the European Union's Horizon 2020 Research and Innovation Program (ERC-2014-StG-633818-dasQ).

*Corresponding author.
shaoxiang.sheng@fmq.uni-stuttgart.de
†Corresponding author.
sebastian.loth@fmq.uni-stuttgart.de

[1] G. S. MacCabe, H. Ren, J. Luo, J. D. Cohen, H. Zhou, A. Sipahigil, M. Mirhosseini, and O. Painter, Nano-acoustic resonator with ultralong phonon lifetime, Science **370**, 840 (2020).

[2] A. A. Maznev, T. C. Hung, Y. T. Yao, T. H. Chou, J. S. Gandhi, L. Lindsay, H. D. Shin, D. W. Stokes, R. L. Forrest, A. Bensaoula, C. K. Sun, and K. A. Nelson, Propagation of THz acoustic wave packets in GaN at room temperature, Appl. Phys. Lett. **112**, 061903 (2018).

[3] S. Hermelin, S. Takada, M. Yamamoto, S. Tarucha, A. D. Wieck, L. Saminadayar, C. Bäuerle, and T. Meunier, Electrons surfing on a sound wave as a platform for quantum optics with flying electrons, Nature (London) **477**, 435 (2011).

[4] I. Robinson and R. Harder, Coherent x-ray diffraction imaging of strain at the nanoscale, Nat. Mater. **8**, 291 (2009).

[5] M. N. Luckyanova, J. Garg, K. Esfarjani, A. Jandl, M. T. Bulsara, A. J. Schmidt, A. J. Minnich, S. Chen, M. S. Dresselhaus, Z. Ren, E. A. Fitzgerald, and G. Chen, Coherent phonon heat conduction in superlattices, Science **338**, 936 (2012).

[6] N. Bonini, J. Garg, and N. Marzari, Acoustic phonon lifetimes and thermal transport in free-standing and strained graphene, Nano Lett. **12**, 2673 (2012).

[7] E. Baldini, A. Dominguez, T. Palmieri, O. Cannelli, A. Rubio, P. Ruello, and M. Chergui, Exciton control in a room temperature bulk semiconductor with coherent strain pulses, Sci. Adv. **5**, eaax2937 (2019).

[8] M. Vinod, G. Raghavan, and V. Sivasubramanian, Fano resonance between coherent acoustic phonon oscillations and electronic states near the bandgap of photoexcited GaAs, Sci. Rep. **8**, 17706 (2018).

[9] M. Stekiel, A. Girard, T. Nguyen-Thanh, A. Bosak, V. Milman, and B. Winkler, Phonon-driven phase transitions in calcite, dolomite, and magnesite, Phys. Rev. B **99**, 054101 (2019).

[10] M. Weiler, H. Huebl, F. S. Goerg, F. D. Czeschka, R. Gross, and S. T. B. Goennenwein, Spin Pumping with Coherent Elastic Waves, Phys. Rev. Lett. **108**, 176601 (2012).

[11] M. Weiler, L. Dreher, C. Heeg, H. Huebl, R. Gross, M. S. Brandt, and S. T. B. Goennenwein, Elastically Driven Ferromagnetic Resonance in Nickel Thin Films, Phys. Rev. Lett. **106**, 117601 (2011).

[12] R. Manenti, A. F. Kockum, A. Patterson, T. Behrle, J. Rahamim, G. Tancredi, F. Nori, and P. J. Leek, Circuit quantum acoustodynamics with surface acoustic waves, Nat. Commun. **8**, 975 (2017).

[13] K. J. Satzinger, Y. P. Zhong, H. S. Chang, G. A. Peairs, A. Bienfait, M. H. Chou, A. Y. Cleland, C. R. Conner, Dumur, J. Grebel, I. Gutierrez, B. H. November, R. G. Povey, S. J. Whiteley, D. D. Awschalom, D. I. Schuster, and A. N. Cleland, Quantum control of surface acoustic-wave phonons, Nature (London) **563**, 661 (2018).

[14] S. Sheng, J. Bin Wu, X. Cong, W. Li, J. Gou, Q. Zhong, P. Cheng, P. H. Tan, L. Chen, and K. Wu, Vibrational Properties of a Monolayer Silicene Sheet Studied by Tip-Enhanced Raman Spectroscopy, Phys. Rev. Lett. **119**, 196803 (2017).

[15] S. Sheng, J. Bin Wu, X. Cong, Q. Zhong, W. Li, W. Hu, J. Gou, P. Cheng, P. H. Tan, L. Chen, and K. Wu, Raman spectroscopy of two-dimensional borophene sheets, ACS Nano **13**, 4133 (2019).

[16] J. Lee, K. Fujita, K. McElroy, J. A. Slezak, M. Wang, Y. Aiura, H. Bando, M. Ishikado, T. Masui, J. X. Zhu, A. V. Balatsky, H. Eisaki, S. Uchida, and J. C. Davis, Interplay of electron-lattice interactions and superconductivity in $Bi_2Sr_2CaCu_2O_{8+\delta}$, Nature (London) **442**, 546 (2006).

[17] D. Peller, L. Z. Kastner, T. Buchner, C. Roelcke, F. Albrecht, N. Moll, R. Huber, and J. Repp, Sub-cycle atomic-scale forces coherently control a single-molecule switch, Nature (London) **585**, 58 (2020).

[18] T. L. Cocker, D. Peller, P. Yu, J. Repp, and R. Huber, Tracking the ultrafast motion of a single molecule by femtosecond orbital imaging, Nature (London) **539**, 263 (2016).

[19] P. Ruello and V. E. Gusev, Physical mechanisms of coherent acoustic phonons generation by ultrafast laser action, Ultrasonics **56**, 21 (2015).

[20] V. Jelic, K. Iwaszczuk, P. H. Nguyen, C. Rathje, G. J. Hornig, H. M. Sharum, J. R. Hoffman, M. R. Freeman, and F. A. Hegmann, Ultrafast terahertz control of extreme tunnel currents through single atoms on a silicon surface, Nat. Phys. **13**, 591 (2017).

[21] T. L. Cocker, V. Jelic, M. Gupta, S. J. Molesky, J. A. J. Burgess, G. D. L. Reyes, L. V. Titova, Y. Y. Tsui, M. R. Freeman, and F. A. Hegmann, An ultrafast terahertz scanning tunnelling microscope, Nat. Photonics **7**, 620 (2013).

[22] M. Abdo, S. Sheng, S. Rolf-Pissarczyk, L. Arnhold, J. A. J. Burgess, M. Isobe, L. Malavolti, and S. Loth, Variable repetition rate THz source for ultrafast scanning tunneling microscopy, ACS Photonics **8**, 702 (2021).

[23] H. Shigekawa, O. Takeuchi, and M. Aoyama, Development of femtosecond time-resolved scanning tunneling microscopy for nanoscale science and technology, Sci. Technol. Adv. Mater. **6**, 582 (2005).

[24] See Supplemental Material at http://link.aps.org/supplemental/10.1103/PhysRevLett.129.043001 for experimental details, calculation of the thermal stress, terahertz-induced voltage in the STM junction, and acoustic phonon modes near a Au step edge, which includes Refs. [18–22,25–36].

[25] T. Andreev, I. Barke, and H. Hövel, Adsorbed rare-gas layers on Au(111): Shift of the Shockley surface state studied with ultraviolet photoelectron spectroscopy and scanning tunneling spectroscopy, Phys. Rev. B **70**, 205426 (2004).

[26] O. B. Wright, Ultrafast nonequilibrium stress generation in gold and silver, Phys. Rev. B **49**, 9985 (1994).

[27] B. M. Law and F. Rieutord, Electrostatic forces in atomic force microscopy, Phys. Rev. B **66**, 035402 (2002).

[28] S. Belaidi, P. Girard, and G. Leveque, Electrostatic forces acting on the tip in atomic force microscopy: Modelization and comparison with analytic expressions, J. Appl. Phys. **81**, 1023 (1997).

[29] M. Garg and K. Kern, Attosecond coherent manipulation of electrons in tunneling microscopy, Science **367**, 411 (2020).

[30] J. Merker, D. Lupton, M. Töpfer, and H. Knake, High temperature mechanical properties of the platinum group metals: Elastic properties of platinum, rhodium and iridium and their alloys at high temperatures, Platinum Met. Rev. **45**, 74 (2001).

[31] M. Müller, N. M. Sabanés, T. Kampfrath, and M. Wolf, Phase-resolved detection of ultrabroadband THz pulses inside a scanning tunneling microscope junction, ACS Photonics **7**, 2046 (2020).

[32] D. B. Dougherty, P. Maksymovych, J. Lee, M. Feng, H. Petek, and J. T. Yates, Tunneling spectroscopy of stark-shifted image potential states on Cu and Au surfaces, Phys. Rev. B **76**, 125428 (2007).

[33] A. Levchuk, B. Wilk, G. Vaudel, F. Labbé, B. Arnaud, K. Balin, J. Szade, P. Ruello, and V. Juvé, Coherent acoustic phonons generated by ultrashort terahertz pulses in nanofilms of metals and topological insulators, Phys. Rev. B **101**, 180102(R) (2020).

[34] J. M. Manceau, P. A. Loukakos, and S. Tzortzakis, Direct acoustic phonon excitation by intense and ultrashort terahertz pulses, Appl. Phys. Lett. **97**, 251904 (2010).

[35] N. Laman and D. Grischkowsky, Terahertz conductivity of thin metal films, Appl. Phys. Lett. **93**, 051105 (2008).

[36] O. B. Wright and K. Kawashima, Coherent Phonon Detection from Ultrafast Surface Vibrations, Phys. Rev. Lett. **69**, 1668 (1992).

[37] A. Castellanos-Gomez, M. Wojtaszek, N. Tombros, N. Agraït, B. J. Van Wees, and G. Rubio-Bollinger, Atomically thin mica flakes and their application as ultrathin insulating substrates for graphene, Small **7**, 2491 (2011).

[38] W. Melitz, J. Shen, A. C. Kummel, and S. Lee, Kelvin probe force microscopy and its application, Surf. Sci. Rep. **66**, 1 (2011).

[39] K. Araki, Y. Ie, Y. Aso, H. Ohoyama, and T. Matsumoto, Time-resolved electrostatic force microscopy using tip-synchronized charge generation with pulsed laser excitation, Commun. Phys. **2**, 10 (2019).

[40] A. Kyndiah, M. Checa, F. Leonardi, R. Millan-Solsona, M. Di Muzio, S. Tanwar, L. Fumagalli, M. Mas-Torrent, and G. Gomila, Nanoscale mapping of the conductivity and interfacial capacitance of an electrolyte-gated organic field-effect transistor under operation, Adv. Funct. Mater. **31**, 2008032 (2021).

[41] H. Wang, L. Wang, D. S. Jakob, and X. G. Xu, Tomographic and multimodal scattering-type scanning near-field optical microscopy with peak force tapping mode, Nat. Commun. **9**, 2005 (2018).

[42] X. Li, D. Chen, M. Jin, D. Ma, Y. Ge, J. Sun, W. Guo, H. Sun, J. Han, W. Xiao, J. Duan, Q. Wang, C. C. Liu, R. Zou, J. Cheng, C. Jin, J. Zhou, J. B. Goodenough, J. Zhu, and Y. Yao, Pressure-induced phase transitions and superconductivity in a quasi-1-dimensional topological crystalline insulator α-Bi_4Br_4, Proc. Natl. Acad. Sci. U.S.A. **116**, 17696 (2019).

[43] K. Cho, M. Kończykowski, S. Teknowijoyo, M. A. Tanatar, J. Guss, P. B. Gartin, J. M. Wilde, A. Kreyssig, R. J. McQueeney, A. I. Goldman, V. Mishra, P. J. Hirschfeld, and R. Prozorov, Using controlled disorder to probe the interplay between charge order and superconductivity in $NbSe_2$, Nat. Commun. **9**, 2796 (2018).